Dissolution from a liquid CO_2 lake disposed in the deep ocean

Ilker Fer[1] and Peter M. Haugan

Geophysical Institute, University of Bergen, Allégaten 70, N-5007, Bergen, Norway

Abstract

The dissolution from a liquid CO_2 lake source located at a flat ocean bottom at 3,000 m depth is investigated. Using the unsteady, two-dimensional advection–diffusion equation, temporal and spatial distribution of CO_2 dissolved from the source of 500 m length and of unit span is sought in a domain of 20 km horizontal and 200 m vertical extent. Different cases were run with uniform longitudinal speed and constant horizontal and vertical diffusion coefficients and with vertical profiles of velocity and diffusivity derived from turbulent boundary layer theory. Each case was run with and without a hydrate film at the interface between the seawater and the liquid CO_2. The properties of the hydrate film are modeled using a capillary permeation model. The computations show that the presence of a hydrate layer retards the dissolution rate by a factor of 2.7 when the density effects due to the increase of CO_2 concentration as a result of the dissolution are neglected. However, the strong, stable stratification above the hydrate layer, as a consequence of the increase in density of seawater enriched by CO_2, suppresses the vertical mixing considerably and reduces the sensitivity to hydrate. The dissolution rate is found to be 0.1 m yr^{-1} for realistic vertical profiles of longitudinal velocity (order of 5 cm s^{-1}) and diffusivity. However, during conditions of a benthic storm (20 cm s^{-1}), the dissolution rate reaches 1.6 m yr^{-1}.

Enhanced emission of greenhouse gases, particularly carbon dioxide (CO_2), to the atmosphere is widely accepted to affect the global climate system (Houghton et al. 1995). The atmospheric CO_2 content at present is about 25% higher than preindustrial levels. Over the past two decades, multidisciplinary research has been intensified with a focus to stabilize the CO_2 level in the atmosphere. One of the potential options to mitigate atmospheric levels is to capture it from fossil fuel combustors and purposefully dispose of and sequester it elsewhere (e.g., in ocean, deep saline aquifers, depleted gas and oil wells, coal beds, etc.). The ocean appears to be a preferable option because it is the largest potential sink for anthropogenic CO_2. Marchetti (1977) was the first to propose ocean disposal to accelerate the natural ocean uptake of atmospheric CO_2. He suggested that efficient long-term sequestration could be achieved through the Gibraltar Strait, where the outflow of dense water cascades to ~1,000 m depth and, in consequence, spreads out in the North Atlantic.

The research on ocean disposal options has mostly focused on predicting the behavior and the dissolution time scale of the released CO_2 and on quantifying the environmental impacts to marine systems (*see,* e.g., Handa and Ohsumi 1995). Different scenarios of CO_2 disposal in the ocean have been proposed at various depths and in different forms in relation to the phase properties of CO_2. The phase diagram for the CO_2–water system shows that when pressure is greater than ~4.5 MPa and the temperature is less than 9.85°C, clathrate-hydrate crystal (hereafter hydrate) develops. Density profiles of liquid CO_2, CO_2-saturated seawater, and seawater are shown in Fig. 1, together with the approximate density of hydrate, condensation depth, and depth at which we might expect hydrate to develop. Because of its large compressibility, liquid CO_2 is relatively denser than seawater at depths greater than ~3,000 m. Liquefied CO_2 released at shallower depths will lead to rising droplet plumes, which, on reaching the condensation depth of ~450 m, will form CO_2 bubbles (Liro et al. 1992). The combined effect of rising droplets and sinking, dense, CO_2-enriched seawater has been simulated recently by Alendal and Drange (2001). Furthermore, dissolution of CO_2 increases the density of water, and it was suggested by Drange et al. (1993) that a gravity current could be achieved toward the deep ocean if sufficiently dense CO_2-enriched water (Haugan and Drange 1992) were released on a sloping bottom. Disposal of liquid CO_2 at depths where it is denser than seawater (>3,000 m) is expected to fill topographic depressions and, in turn, accumulate as a large lake of CO_2 (Ohsumi 1993) over which a thin hydrate layer forms and retards the dissolution. The hydrate films are not perfect insulators against the interliquid-phase CO_2 transfer, and they are continuously "metabolized" through decomposition of aged crystals and formation of new crystals (Mori 1998). The dissolved CO_2 diffuses out into the benthic boundary layer, where advection and mixing takes place because of currents and turbulence near the bottom.

In this paper, we address the option of CO_2 disposal as a lake in the deep ocean. We attempt to envisage the fate of the liquid CO_2 pool through simple numerical simulations of the two-dimensional (2D) advection–diffusion equation, incorporating the bottom boundary layer dynamics and the effects of the hydrate layer. First, the CO_2–seawater system, including hydrates, then salient features of bottom boundary layer dynamics, is described. Subsequently, the numerical model and results are presented. In the discussion section, we also address instability at the hydrate interface and gravity current dynamics. A notation list is provided in Table 1.

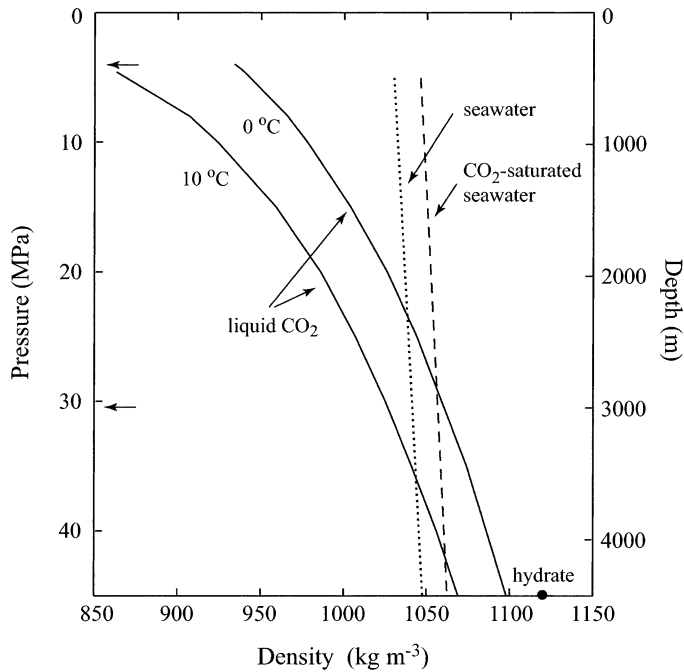[1] Corresponding author (ilker.fer@gfi.uib.no).

Fig. 1. Density profiles of liquid CO_2 at 0°C and 10°C (solid curves), CO_2-saturated seawater (dashed line), and seawater (dotted line). Densities of seawater and CO_2-saturated seawater are calculated for $T = 5$°C and $S = 35$ using the international equation of state (UNESCO 1981) and Eq. 15, which incorporates the effect of dissolved CO_2 concentration, respectively. Densities for liquid CO_2 are given by Vukalovich and Altunin (1968). The approximate density of hydrate (Udachin et al. 2001) is shown by the dot on the density axis. The phase boundaries for gas–liquid CO_2 transition (i.e., condensation pressure) and for hydrate formation at 5°C are shown by the uppermost and lowermost arrows on the pressure axis, respectively. Depth is calculated from pressure.

CO₂–seawater system

Hydrate formation at liquid CO_2–water interface—CO_2 hydrate, a binary clathrate compound, forms when the cavities of hydrogen-bonded structures are occupied by CO_2 molecules. The chemical formula yields $CO_2 \cdot n \cdot H_2O$ where n is the hydration number, and if all the cavities are occupied $n = 5.75$. Several researchers used the maximum value (1,130 kg m^{-3}) of the hydrate density, which is estimated from the perfect crystallographic lattice formation and the full occupancy of CO_2 molecules into clathrate cages. However, the CO_2 hydrate formed under arbitrary conditions can yield various densities (Uchida 1997). Udachin et al. (2001) recently estimated the density of CO_2 hydrate as 1,120 ± 10 kg m^{-3} for a calculated lattice constant at 4°C and a composition of $CO_2 \cdot 6.20 \cdot H_2O$. Here, the main estimated uncertainty arises from the cage occupancies. At depths considered for direct disposal of CO_2 in the deep ocean, ~3,000 m, the hydrostatic pressures will be as high as ~30.5 MPa, and the composition will tend toward complete filling of the cages (Udachin et al. 2001). For the stability of a CO_2 lake, a better knowledge of the buoyancy behavior of the CO_2 hydrates, hence its density, and of its mechanical properties is required.

Table 1. Notation. Unit abbreviations are M, mass; L, length; T, time.

Symbol	Unit	Parameter
A	L^2	Surface area
C	mol L^{-3}	Concentration
C$_D$	—	Drag coefficient
C$_S$	mol L^{-3}	Solubility of CO_2 in seawater
$\tilde{C}_S$	—	Solubility of CO_2 in seawater as a mole fraction
d	L	Height of roughness elements
D	L^2 T^{-1}	Molecular diffusivity of CO_2 in water
f	T^{-1}	Coriolis parameter
F	M L^{-1} T^{-2}	Fugacity
g	L T^{-2}	Acceleration due to gravity
h	L	BBL thickness
J	mol L^{-2} T^{-1}	Molar flux
k	L^{-1}	Wave number
K$_m$	L T^{-1}	Mass transfer coefficient
K$_x$, K$_z$	L^2 T^{-1}	Horizontal and vertical diffusivities
M	M mol^{-1}	Molar mass
n	—	Hydration number
N	T^{-1}	Buoyancy frequency
p	—	Porosity
P	M L^{-1} T^{-2}	Pressure
r$_c$	L	Radius of capillary
Re$_*$	—	Roughness Reynolds number
S	—	Salinity
Sc	—	Schmidt number
t	T	Time
T	°C	Temperature
U	L T^{-1}	Velocity
u$_*$	L T^{-1}	Friction velocity
V$_p$	L T^{-1}	Piston velocity
z	L	Vertical distance
z$_0$	L	Roughness parameter
δ	L	Hydrate film thickness
δ$_E$	L	Ekman boundary layer thickness
ε	L^2 T^{-3}	Dissipation rate of TKE
φ	degrees	Contact angle
γ	M T^{-2}	Surface tension
Γ	—	Mixing efficiency
η	M L^{-1} T^{-1}	Absolute viscosity
κ	—	von-Karman's constant
λ	L	Wave length
ν	L^2 T^{-1}	Kinematic viscosity
θ	K	Absolute temperature
ρ	M L^{-3}	Density
τ	—	Tortuosity
τ$_0$	M L^{-1} T^{-2}	Shear stress at the bottom
$\bar{\nu}$	L^3 mol^{-1}	Partial molar volume

Deep-sea disposal of CO_2 is certain to lead to CO_2 hydrate formation (Brewer et al. 1999). Naturally occurring CO_2 clathrate hydrates were observed by Sakai et al. (1990) during a submersible study. CO_2-rich fluid bubbles emerging from the sea floor at 1,335 to 1,550 m depth in the mid-Okinawa Trough immediately formed hydrates on contact with 3.8°C seawater, which in turn developed fragile hydrate tubes standing on the sediments. The observations were followed by in situ experiments, notably by Honda et al. (1995), who observed the changes of initially solid CO_2 contained in a cylinder while they lowered it to 3,073 m depth

by a manned submersible, and those by Brewer et al. (1999), who reported intermittent overflows of liquid CO_2 and massive hydrate formation from a beaker, initially half full with CO_2, disposed of on the ocean floor at 3,627 m depth. Brewer et al. (1999) observed that the pool of liquid CO_2 on the seafloor expanded in volume more than four times, forming hydrate, which eventually dissolved. Recently, the dissolution rate of liquid CO_2 that is accumulated into a small hole made by a push core on the ocean floor at 3,600 m depth and 1.55°C was directly measured by Dunk et al. (unpubl.) using a remotely operated vehicle (ROV) and a pH electrode. Their estimate of 1.7 μmol cm^{-2} s^{-1} is comparable to the dissolution rate of 3 μmol cm^{-2} s^{-1} determined from the shrinking rate of a rising stream of CO_2 droplets at 800 m depth (Peltzer et al. 2000). On a subsequent note, Peltzer et al. (unpubl.) reported on a massive "frost-heave," which formed at one of the corrals at 3,604 m, whereas a similar corral nearby showed no such behavior.

Various aspects of the structure and composition of the hydrate are studied by spectroscopic and diffraction measurements (*see*, e.g., Udachin et al. 2001) and the modeling of clathrate hydrate formation at the interface between liquid CO_2 and water is extensively reviewed by Mori (1998). Mori, in his review, classified hydrate film models into three different groups: diffusive suspension layer models (e.g., Shindo et al. 1995), permeable solid plate models (e.g., Teng et al. 1996*b*), and sediment particle aggregate layer model (Inoue et al. 1996). Laboratory experiments simulating CO_2 disposal in the deep ocean showed that the hydrate phase that grows at the interface between liquid CO_2 and water is very thin (order of μm) but rather stable (Shindo et al. 1995). The hydrate film never prevents, but only retards, the interphase mass transfer of CO_2, provided the water phase is not saturated with CO_2. The dissolution mechanism being retarded through the hydrate film, the so-called "barrier effect," has been discussed by Mori and Mochizuki (1998).

Solubility of carbon dioxide in seawater—A reliable estimate of the fate of purposefully discharged or stored CO_2 in the ocean requires calculation of CO_2 solubility in seawater. In order to account for the nonideality of CO_2, it was proposed to employ a modified Henry's law by expressing the activity of the solute in the gas phase by its fugacity, F, and by correcting the thermodynamic expansion of the solution by the dissolved gas. King (1969) presents a thorough discussion of Henry's law and its application to real gasses over a wide range of pressures. According to the modified Henry's law, the solubility of CO_2 in liquids with elevated pressures up to 50 MPa can be represented as $C_s = K_0 F[\exp(P_0 - P)\bar{\nu}/R\theta]$. Here K_0 is known as the modified Henry's law constant or solubility coefficient, F is the fugacity, P is the pressure, $P_0 \sim 0.1$ MPa is the atmospheric pressure, $\bar{\nu}$ is the partial molar volume of CO_2, R is the gas constant, and θ is the absolute temperature. K_0 depends on temperature and salinity (Weiss 1974). We have evaluated F for the gas and the liquid phase using a relation derived by Teng et al. (1996*a*) that incorporates a Benedict–Webb–Rubin equation of state (Bishnoi and Robinson 1971; Weiss 1974). In the calculation of F and C_s in the gas phase, the system pressure, P, has to be replaced by the condensation
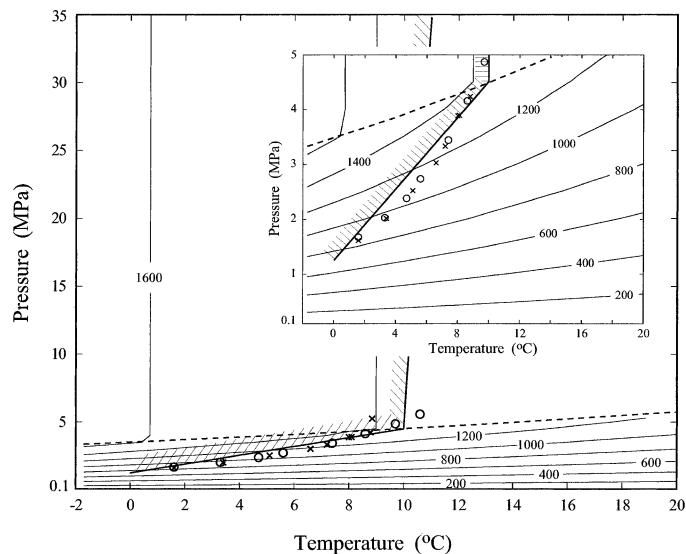

Fig. 2. Solubility of CO_2 in seawater with $S = 35$ (contours, mol m^{-3}). The dashed line is the condensation line (i.e., the boundary between gaseous and liquid phases of pure CO_2) and is obtained by a curve fit to data points of Lide (2000). The rough limit for hydrate formation in pure water is represented by the hatched area using the data given by King (1969). The phase boundary for hydrate formation in seawater is depicted by circles (Mitsubishi 1990) and crosses (Ohgaki et al. 1993). The inset shows solubility in the pressure range 0.1–5 MPa for clarity.

pressure for pure CO_2, which can be estimated as a function of temperature by a curve fit to the data points of Lide (2000).

Solubility of CO_2 in seawater is shown in Fig. 2. The calculated values are converted to mole fraction of CO_2, $\tilde{C}_s$, in the entirety of the given CO_2–water system and are compared to those given by Stewart and Munjal (1970) in Fig. 3. In both figures, available data in the literature that cover wide pressure and temperature ranges are compared with the calculations. It should be noted that even at pressures favoring hydrate formation, data were obtained in the absence of hydrate. C_s in seawater coexisting with the hydrate phase was reported only recently, notably by Aya et al. (1997). Solubility data measured by them at 30 MPa at the presence of hydrate are also shown in Fig. 3.

Dynamics near the ocean bottom

Bottom boundary layer and turbulence—The fate of a CO_2 lake disposed in the deep ocean will predominantly depend on the dynamics associated with the boundary layer near the ocean bottom and the consequent turbulence characteristics. A bottom boundary layer (BBL), a well-mixed layer vertically uniform in potential temperature, salinity, and light scattering, has been observed over large regions of the deep ocean (Armi and Millard 1976; D'Asaro 1982). The BBL is typically bounded by a sharp interface of strong vertical temperature, salinity and density gradients underlying a uniformly stratified region (Armi 1977). It was first suggested by Munk (1966) and later confirmed by Armi (1978) that mixing near the bottom might be responsible for a sig-
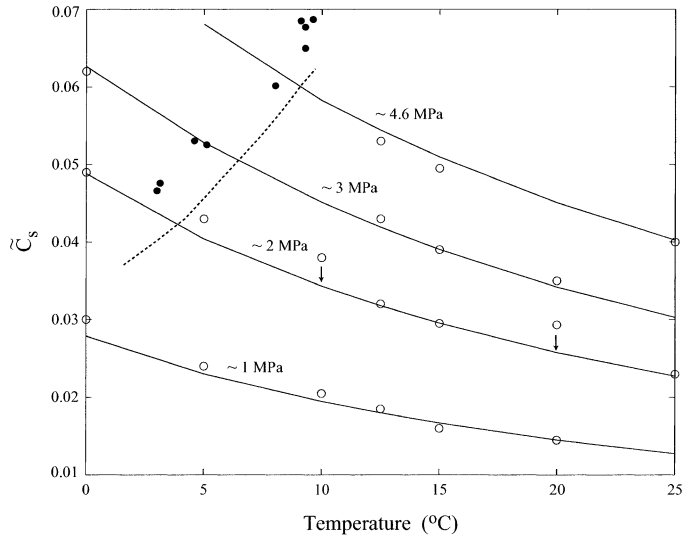
Fig. 3. Solubility of CO_2 as a mole fraction in seawater. The hydrate formation boundary (dashed line) is after Ohgaki et al. (1993). Solid curves are obtained after calculating the solubility for $S = 35$. Open circles represent experimental data compiled by Stewart and Munjal (1970) from several different sources. Arrows show that the two outliers belong to the ~2 MPa data set. Dots indicate data obtained by Aya et al. (1997) at 30 MPa in the presence of hydrate.

nificant part of the vertical transport of buoyancy and tracers in the abyssal ocean. The concept has recently received a considerable amount of observational support (Thorpe et al. 1990; Toole et al. 1997; Ledwell et al. 2000) and theoretical attention (Thorpe 1987; Garrett 1990, 2001).

Turbulence in the boundary layer is thoroughly studied (*see,* e.g., Hinze 1975), and the oceanic BBL turbulence is widely accepted to be similar to that observed in laboratory flumes, provided the lowermost 1–2 m of the benthic BBL is independent of Coriolis effects (Wimbush and Munk 1970). The thickness of the BBL is often taken to be about the Ekman boundary layer thickness, δ_E, commonly expressed by the relation in Eq. 1.

$$\delta_E = \frac{\kappa u_*}{f} \qquad (1)$$

$\kappa = 0.41$ is the von-Karman's constant, u_* is the friction velocity, and f is the Coriolis parameter. For a steady, turbulent boundary layer driven by a geostrophic flow, U, the friction velocity is typically estimated to be equal to $U/30$ (Weatherly 1975). Introducing $U = 0.05$ m s⁻¹, $f = 10^{-4}$ s⁻¹, Eq. 1 yields $\delta_E \sim 6.6$ m—considerably less than generally observed values of BBL thickness (Armi and Millard 1976; D'Asaro 1982). On dimensional grounds, Weatherly and Martin (1978) proposed an expression for δ_E that incorporates the stratification of the fluid.

$$\delta_E = A \frac{u_*}{f[1 + (N/f)^2]^{1/4}} \qquad (2)$$

A is a constant and the buoyancy frequency in the interior, N, is approximated by Eq. 3.

$$N = \left(\frac{g}{\rho_0} \frac{\partial \rho}{\partial z} \right)^{1/2} \qquad (3)$$

Weatherly and Martin (1978) report that the BBL thickness is fairly well approximated over the range $0 \leq N/f \leq 200$, provided that $A = 1.3$.

In the lower part of the BBL, forces induced by shear are greater than those induced by buoyancy and Coriolis effects, and the structure is similar to the "wall region" of a non-rotating boundary layer where the vertical velocity distribution can be described by the logarithmic profile.

$$U(z) = \frac{u_*}{\kappa} \ln \frac{z}{z_0} \qquad (4)$$

z_0 is a roughness parameter equal to $0.11\nu/u_*$ for a smooth bottom. The roughness of the bottom can be described in terms of a roughness Reynolds number, $Re_* = u_* d/\nu$, where d is the height of the roughness elements. The regime is considered to be hydraulically smooth for $Re_* < 5$. For the present purposes, if we consider a mean flow of 0.05 m s⁻¹ over a CO_2 lake covered by a hydrate layer of thickness on the order of 10^{-5} m (*see* "The model") and assume that the height of the roughness elements is on the order of the hydrate layer thickness, we obtain $Re_* \approx 10^{-2}$ using $\nu \approx 10^{-6}$ m² s⁻¹. Therefore, the flow over the CO_2 lake can be considered hydraulically smooth. Assuming the "law of the wall" is applicable, which is typically the case for smooth flow over fine sediments in lakes and oceans, the dissipation rate of turbulent kinetic energy, ε, as a function of distance from the wall, z, scales as

$$\varepsilon(z) = \frac{\tau_0}{\rho} \frac{\partial U}{\partial z} = \frac{u_*^3}{\kappa z} \qquad (5)$$

where the bottom shear stress $\tau_0 = u_*^2 \rho$ is used.

Horizontal and vertical diffusivity—Assuming isotropy and a stationary balance between the buoyancy flux and the dissipation of turbulent kinetic energy, ε, Osborn (1980) has proposed a scaling for the vertical diffusivity of the form

$$K_z = \Gamma \frac{\varepsilon}{N^2} \qquad (6)$$

where Γ is the mixing efficiency, and the buoyancy frequency N is given by Eq. 3. Γ indicates the conversion efficiency of turbulent kinetic energy into potential energy of the system and is commonly taken to be 0.2 for oceanic stratified turbulence. A range of estimates of Γ are found and used in the literature. Lilly et al. (1974) obtained $\Gamma = 0.33$ from atmospheric measurements. Oakey (1982) estimated $\Gamma = 0.26 \pm 0.21$ using dissipation rate calculations from the high–wave number cutoff of the temperature microstructure spectra from oceanic waters. Fer et al. (2002*a*) observed $\Gamma = 0.15 \pm 0.1$ in the upper mixed layer and 0.22 ± 0.2 near the sloping sides of Lake Geneva, both comparable to the values found in the ocean interior.

Clauser (1956) suggested that the vertical eddy diffusion at the upper boundary of the BBL can be estimated by

$$K_z \approx \frac{1}{15} u_* h \qquad (7)$$

where h is the height of the BBL, and u_* is the friction velocity. Assuming $U/u_* = 30$, a mean velocity of $U = 10$ cm s^{-1}, and $h = 50$ m, Eq. 7 gives $K_z \approx 10^{-2}$ m^2 s^{-1}. This is a very rough estimate, and it was pointed out by Armi (1977) that very little is known about the turbulence within the BBL and above the Ekman layer. He suggested that roll waves, or intermittent surges, can form when the internal Froude number (ratio of the mean velocity of the current to the velocity of a long wave at the interface) of the flow is above a critical value ($\sim$1.7 for a flat bottom). Similar interfacial instabilities were observed on sloping sides of a deep lake (Fer et al. 2001, 2002b). Compared to the ocean interior, relatively large eddy diffusivities have been observed; for example, Polzin et al. (1996) reported an average of $K_z = 1.5 \times 10^{-2}$ m^2 s^{-1} for water below 4,000 m within the Romanche fracture zone and downstream of the main sill, whereas estimated K_z at middepth in the vicinity was about 2×10^{-5} m^2 s^{-1}. Enhanced mixing was observed over rough topography in the abyssal ocean, where measurements of tracer dispersion and turbulent energy dissipation in the Brazil Basin revealed diffusivities of $2–4 \times 10^{-4}$ m^2 s^{-1} at 500 m above the abyssal hills on the flank of the mid-Atlantic ridge and $\sim$10^{-3} m^2 s^{-1} nearer the bottom (Ledwell et al. 2000).

Stable density stratification can strongly influence the turbulent boundary layer and, for sufficiently large values of N, can suppress the turbulence completely (Turner 1973). This has to be kept in mind, particularly with respect to strong stable density gradients induced by the dissolution of liquid CO_2 in seawater resulting in large buoyancy frequencies. Furthermore, sediment concentration, if large enough, can alter the dynamics significantly. Turbulence then acts against the gravitational forces tending to resettle the sediments, which are likely to be suspended (e.g., during a benthic storm).

Horizontal diffusivity can be written as

$$K_x = Ahu_* \tag{8}$$

where A is a constant, and h is the depth in open-channel flows or the relevant vertical length scale (BBL thickness, here). Experiments in turbulent open-channel flows, as well as field measurements, suggest that A varies greatly within the range 1–7,500 (Fischer 1973). A value for K_x of O(10^2) m^2 s^{-1} can be estimated for a mean flow of 0.05 m s^{-1}, provided A = 600 and $h = 100$ m. On the Madeira Abyssal Plain at a depth of 5,300 m, Saunders (1983) has observed abyssal diffusivities of 250 m^2 s^{-1} and 150 m^2 s^{-1} for East and North directions, respectively.

The model

Temporal and spatial distribution of CO_2 dissolved from a lake source in the deep ocean can be described by the unsteady, 2D advection–diffusion equation (Eq. 9), which can be written in Cartesian coordinates.

$$\frac{\partial C}{\partial t} + \frac{\partial(uC)}{\partial x} + \frac{\partial(wC)}{\partial z} = \frac{\partial}{\partial x}\left(K_x\frac{\partial C}{\partial x}\right) + \frac{\partial}{\partial z}\left(K_z\frac{\partial C}{\partial z}\right) \tag{9}$$

Here, C is the concentration of CO_2, and u and w are the components of velocity in the horizontal direction x and the vertical direction z, respectively. K_x and K_z are the corresponding horizontal and vertical diffusivities. We define a domain of 20 km horizontal and 200 m vertical extent located at a flat ocean bottom at 3,000 m depth in which there is a lake of CO_2 of 500 m length and unit span 1,500–2,000 m from the origin. Because this is an idealized model study where we focus on fundamental interactions between the CO_2 lake, hydrate, and BBL structure, we restrict ourselves to a flat bottom and a 2D approach with no variability in the y direction perpendicular to the specified horizontal currents. Strictly speaking, the solutions represent a line source of infinite width in the y direction. In a three-dimensional configuration with finite source width, cross-flow dilution would reduce the concentration downstream in the outer parts of the domain. However, the 2D solutions obtained here should be representative of the peak concentrations downstream of a finite width source for a length scale of several times the source width. The time evolution of the solution to Eq. 9 is sought using a finite volume method (*see,* e.g., Ferziger and Perić 1999), with an upwind differencing scheme for spatial and a Crank–Nicolson method for temporal discretization. An equidistant grid yielding 250- and 5-m (1.25-m when h = 25 m) resolution horizontally and vertically, respectively, is employed, and a strongly implicit procedure (SIP) solver is used with a convergence error reduced to $<$10^{-5}. The time step is chosen to satisfy the condition of numerical stability for each of the varying cases (typically 300 and 60 s for cases with $U = 0.05$ and 0.20 m s^{-1}, respectively). At the ocean floor ($z = 0$), a no-slip condition is imposed on the velocity, and there is no concentration flux through the ocean floor except from the source area. A continuative boundary condition (i.e., zero normal derivatives for all quantities) is used at the outflow boundary. In low-speed and incompressible flows, disturbances introduced at an outflow boundary can have an effect on the entire computational region. However, we have chosen our domain such that the outlet boundary is 18 km away from the source to minimize this effect. A steady flow of the dissolved CO_2 plume with constant propagation rate is achieved typically within hours after the commencement of each simulation. Experiments are terminated before the outflow boundary at $x = 20$ km is reached.

The hydrate film is modeled using the capillary permeation model of Mori and Mochizuki (1997). They assume a steady state and a uniform hydrate layer with thickness δ in which the formation and the dissociation of the hydrate crystals are controlled by the rate of water permeation through capillaries and the rate of diffusive removal of CO_2 molecules from the water-side surface, respectively. Mori and Mochizuki obtained Eq. 10 for the hydrate film thickness.

$$\delta = \frac{r_c p}{\tau^2}\frac{\gamma \cos \phi}{4\eta_{mix}nK_m}\frac{(1 - \tilde{C}_S)^2 + n\tilde{C}_S^2}{\tilde{C}_S - \tilde{C}_{amb}} \tag{10}$$

p is the porosity of the hydrate film, γ is the liquid CO_2–water interfacial tension, τ ($\geq$1) is the tortuosity of the capillaries, ϕ is the water-side contact angle on the capillary wall, η_{mix} ($\sim$1.48 $\times$ 10^{-3} Pa·s) is the viscosity of seawater saturated with CO_2, n is the hydration number and K_m is the mass transfer coefficient. The concentration of CO_2 in the
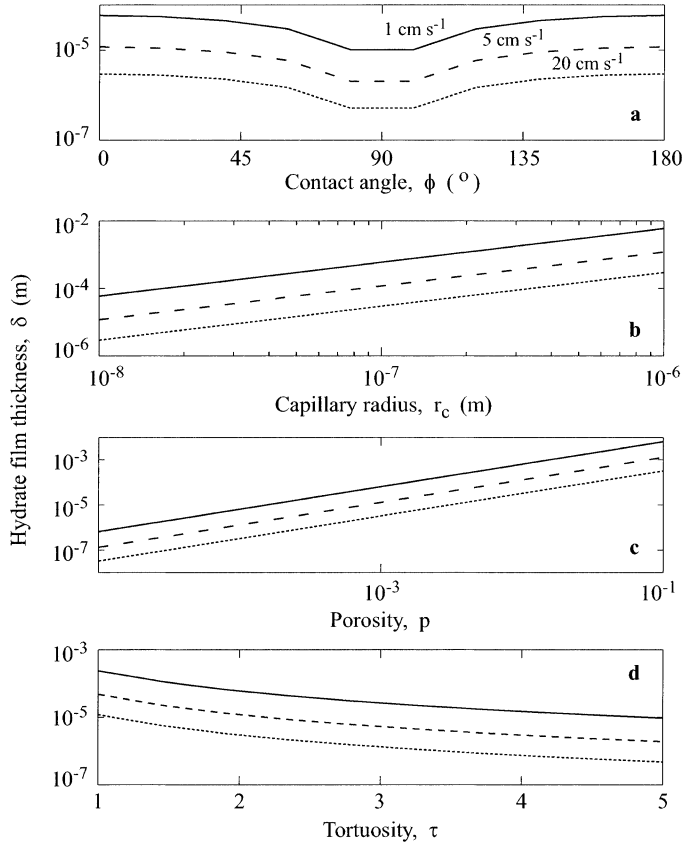
Fig. 4. Dependence of the hydrate film thickness on (a) the contact angle, (b) the capillary radius, (c) the porosity, and (d) the tortuosity. The mean flow over the hydrate layer is 1 (solid line), 5 (dashed line), and 20 cm s⁻¹ (dotted line).

Table 2. Summary of the cases.*

Case	u (m s⁻¹)	K_x (m² s⁻¹)	K_z (m² s⁻¹)	Density effect
1, 1H	0.05	10	0.01	Neglected
2, 2H	BBL†	10	BBL†	Neglected
3, 3H	0.20	10	0.01	Neglected
4, 4H	BBL‡	Eq. 8	BBL‡	Considered
5, 5H	BBL§	Eq. 8	BBL§	Considered

* In all cases, $w = 0$.
† Boundary layer theory is used to derive the vertical distribution of velocity u and K_z for constant N. The ambient velocity above the boundary layer is chosen as 0.05 m s⁻¹. The mixing efficiency, $\Gamma = 0.15$.
‡ Same as footnote † but N is calculated considering the density change effects due to dissolution of CO_2.
§ Same as footnote ‡ but the ambient velocity above the boundary layer is chosen as 0.20 m s⁻¹. $\Gamma = 0.25$.

$$K_m = 0.1u_*Sc^{-0.67} \qquad (14)$$

where $Sc = \nu/D$ is the Schmidt number—O(1,000) for a CO_2–seawater system—and D is the molecular diffusivity of CO_2 in seawater.

In our calculations of the cases when a hydrate layer is present above the CO_2 lake, we used the parameter values of tortuosity, $\tau = 2$; porosity, $p = 10^{-3}$; hydration number, $n = 5.75$; capillary radius, $r_c = 10^{-8}$ m; interfacial tension, $\sigma = 19.4 \times 10^{-3}$ N m⁻¹; and contact angle, $\phi = 0°$. The dependence of the hydrate film thickness on each of the parameters is depicted in Fig. 4 for mean flow speeds of 0.01, 0.05, and 0.20 m s⁻¹. The above parameter values are retained in the calculations, whereas the one corresponding to the relevant panel in Fig. 4 is changed accordingly.

Results

Summary of cases—A total of 10 cases, summarized in Table 2, were simulated. In cases 1–5, it is assumed that no hydrate was formed at the interface between the liquid CO_2 lake and the seawater. Each case is repeated with a hydrate film present and is denoted by H following the number (e.g., case 1H). In the absence of hydrate, the source concentration is set to 1,500 mol m⁻³, which is approximately the solubility at the corresponding depth with $T = 5°C$ and $S = 35$ (Fig. 2). In the presence of hydrate, the hydrate layer is modeled and coupled to the mean flow through Eqs. 10–14. The values of the parameters τ, p, n, r_c, σ, and ϕ given above are retained for all cases in which hydrate is present. Following Ohsumi et al. (1992), the thickness of the BBL for cases 1–3 is taken as $h = 100$ m, which is about 14 times the Ekman layer thickness, δ_E, obtained from Eq. 1 for $f = O(10^{-4})$ s⁻¹. This is certainly an overestimate, except in the case of benthic storms; however, h is set to 25 and 100 m for cases 4 and 5, which is about $4\delta_E$, in agreement with oceanic observations (Armi and Millard 1976; D'Asaro 1982). The vertical diffusivity above the BBL is 10^{-5} m² s⁻¹, typical of the ocean interior (Toole and McDougall 2001). The effects of density change by the dissolution of CO_2 are considered only for cases 4 and 5.

In case 1, the solution to Eq. 9 is sought for a constant longitudinal velocity of $U = 0.05$ m s⁻¹. Vertical and hori-
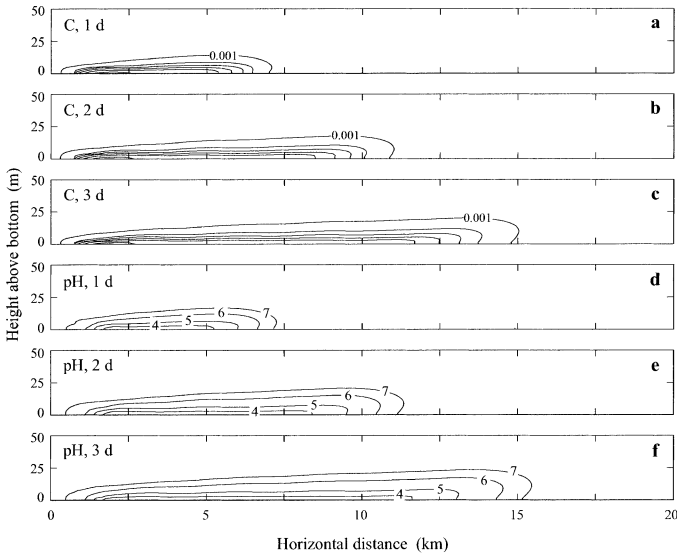
ambient water (bulk of the water phase), $\tilde{C}_{amb}$ (typically several tens of micromoles per kilogram), is negligible compared to $\tilde{C}_S$. The thickness of the hydrate film is inversely proportional to the mass transfer coefficient K_m, which is proportional to the flow above the interface. In consequence, this suggests that δ might vary with bottom currents. Furthermore, molar flux of liquid CO_2 into the water, J_{CO_2}, can be written as Eq. 11.

$$J_{CO_2} = \frac{1}{1 - \tilde{C}_S}\left[K_m\frac{\rho_{mix}}{M_{mix}}(\tilde{C}_S - \tilde{C}_{amb}) - \frac{\tilde{C}_S}{1 - \tilde{C}_S}J_w\right] \quad (11)$$

M_{mix} and ρ_{mix} are the effective molar mass and the density of CO_2-saturated seawater, respectively. The flux of water through the hydrate film, J_w can be calculated as

$$J_w = \frac{r_c p}{\tau^2}\frac{\gamma\cos\phi}{4\delta M_{mix}\nu_{mix}}(1 - \tilde{C}_S) \qquad (12)$$

where ν_{mix} (~1.3 × 10⁻⁶ m² s⁻¹) is the kinematic viscosity of seawater saturated with CO_2. M_{mix} is defined as

$$M_{mix} = M_w(1 - \tilde{C}_S) + M_{CO_2}\tilde{C}_S \qquad (13)$$

where the molar mass of seawater M_w can be estimated as 0.023 kg mol⁻¹ and the molar mass of CO_2, M_{CO_2} is ~0.044 kg mol⁻¹. The mass transfer coefficient can be estimated by

Fig. 5.   Evolution of (a–c) CO_2 concentration, *C*, distribution and the corresponding (d–f) pH distribution for case 4. The contours are drawn at 0.001, 0.007, 0.02, 0.06, 0.2, 0.7, and 1.2 mol L^{-1} (i.e., approximately equal logarithmic space) for *C* and at one-unit intervals for pH. The CO_2 lake source is located 1.5–2 km from the origin.

Fig. 6.   Same as Fig. 5 but for case 4H.

zontal eddy diffusivities are constant and equal to 10^{-2} and 10 m^2 s^{-1}, respectively. These values are comparable to those reported in the literature (*see* the discussion after Eq. 7) and agree well with Eqs. 7 and 8. In case 2, we derive a vertical distribution for the longitudinal velocity using Eq. 4 with a mean geostrophic velocity of 0.05 m s^{-1} above the BBL. A vertical profile for vertical diffusivity, K_z, is calculated using Eq. 6 with $\Gamma = 0.15$ and a constant value for $N = 7 \times 10^{-4}$ s^{-1}, after obtaining an ε profile from Eq. 5. In case 3, we examine the effects of a benthic storm with $U = 20$ cm s^{-1}, which is a typical value for observed benthic storms (*see* "Discussion"). In cases 4 and 5, a density increase from the dissolution of CO_2 is incorporated through a buoyancy frequency profile calculated from Eq. 3. The density of seawater with dissolved CO_2, ρ_2, is calculated by the relation given by Giggenbach (1990) in Eq. 15.

$$\rho_2 = \frac{1,000 + C}{7.5 \times 10^{-4}C + (1,000/\rho_1)} \qquad (15)$$

ρ_1 is the density of seawater without dissolved CO_2 (UNESCO 1981), and *C* is the concentration of dissolved CO_2 (here, g kg^{-1}). The mean velocity above the BBL is set to 0.05 m s^{-1} for case 4 and to 0.20 m s^{-1} for case 5. The vertical distribution for the longitudinal velocity is derived using Eq. 4. In the calculation of the vertical diffusivity profile, Γ is taken as 0.15 and 0.25 for cases 4 and 5, respectively. Horizontal diffusivity is calculated using Eq. 8 with A = 600.

At each time step, the corresponding pH ($= -\log[H^+]$) field is calculated in total scale for added CO_2 concentration to the ambient water having $T = 5°C$, $S = 35$, $P = 30$ MPa, and a constant alkalinity of 2.35 equiv. m^{-3}. The latter fol-lows from assuming negligible dissolution of CaCO$_3$ sedi-
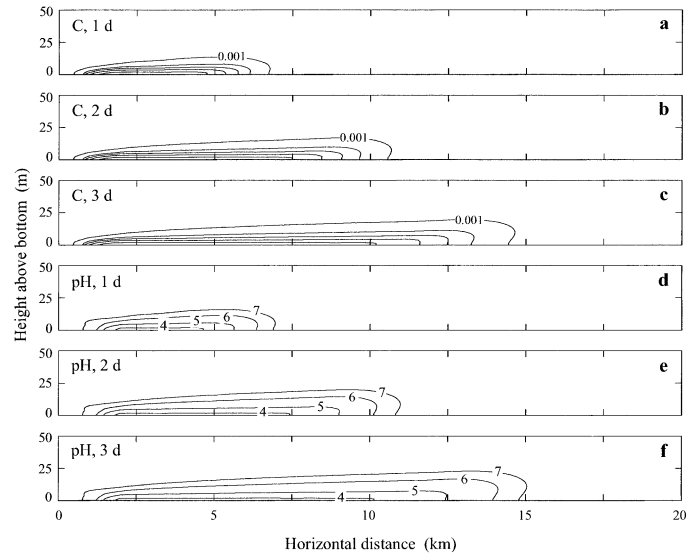
ments. The boric acid system is included in the computa-tions. The ambient water has a pH level of ~7.9 at the corresponding pressure. The pH field calculation is con-ducted in the same fashion for all cases. The time evolution of the concentration, *C,* and the pH for cases 4 and 4H are shown in Figs. 5 and 6, respectively, for 1, 2, and 3 d. The time evolution for the benthic storm cases 5 and 5H are shown in Figs. 7 and 8 for 12 h and 1 d. Because of large longitudinal velocity, the plume of CO_2 reaches the outlet boundary typically after 1 d, compared to >3 d for the cases without the benthic storm.

Vertical distributions of density, ρ; buoyancy frequency, *N*; and vertical diffusivity, K_z for case 4H are shown and compared to those of case 5H in Fig. 9, both at the center of the CO_2 lake and 10 km from the origin. Enhanced CO_2 concentration close to the ocean bottom (i.e., close to the source) results in relatively high values of *N,* which in turn yields suppressed K_z through Eq. 6.
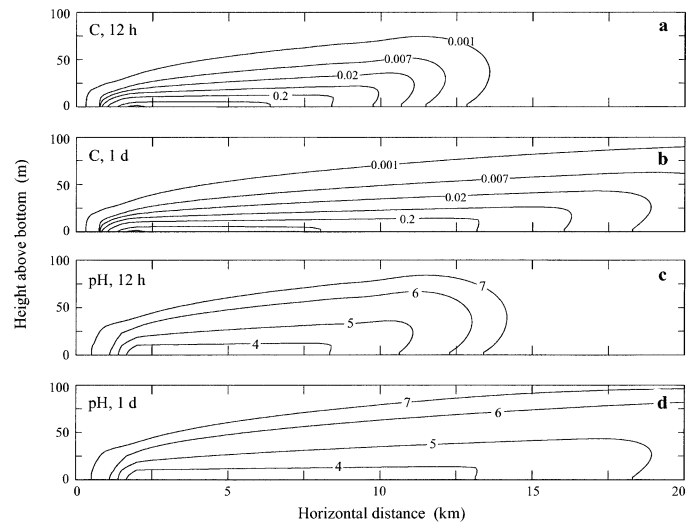

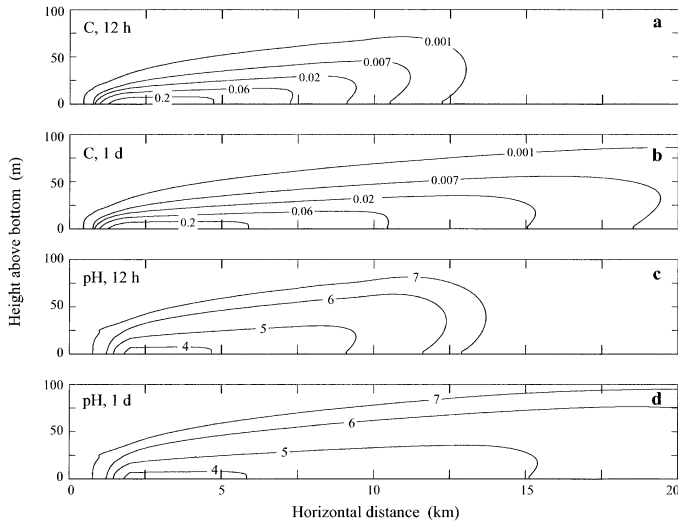Fig. 7.   Same as Fig. 5 but for case 5.

Fig. 8. Same as Fig. 5 but for case 5H.

The total volume of water with pH < 6 is calculated, and its increase with time is shown in Fig. 10 for all cases.

Estimates of the time of complete dissolution—The time variation of the mass of CO_2 stored in the CO_2 lake can be given as Eq. 16.

$$\frac{dW_{CO_2}}{dt} = V_p A(C_{amb} - C_0)M_{CO_2} \qquad (16)$$

W_{CO_2} is the total weight of the CO_2 lake, V_p is the piston velocity (which serves as an effective mass transfer coefficient), M_{CO_2} is the molar mass of CO_2, C_0 is the concentration
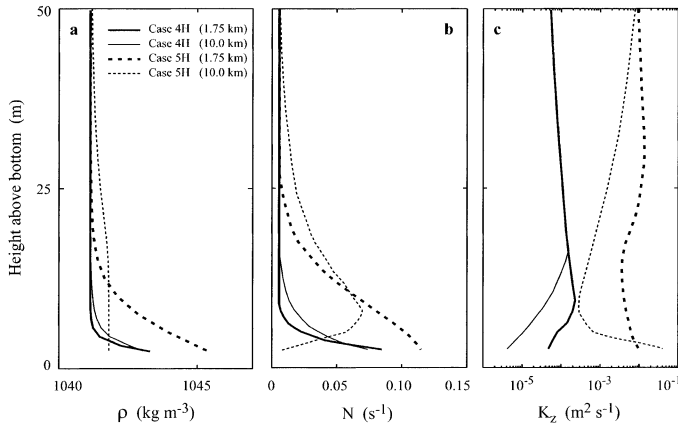

Fig. 9. Vertical distribution of (a) density, ρ; (b) buoyancy frequency, N; and (c) vertical diffusivity, K_z, for case 4H (solid lines) and case 5H (dotted lines). The thick lines are distributions at 1.75 km from the origin (i.e., at the center of the CO_2 lake), whereas thin lines are derived at 10 km from the origin. The profiles are obtained at 3 d for case 4H and at 1 d for case 5H (i.e., when the CO_2 plume approximately reaches the outlet boundary). The density is calculated using Eq. 15 after the CO_2 distribution is obtained. Enhanced CO_2 concentration close to the ocean bottom (i.e., close to the source) results in relatively high values of N, which in turn yields suppressed K_z through Eq. 6.
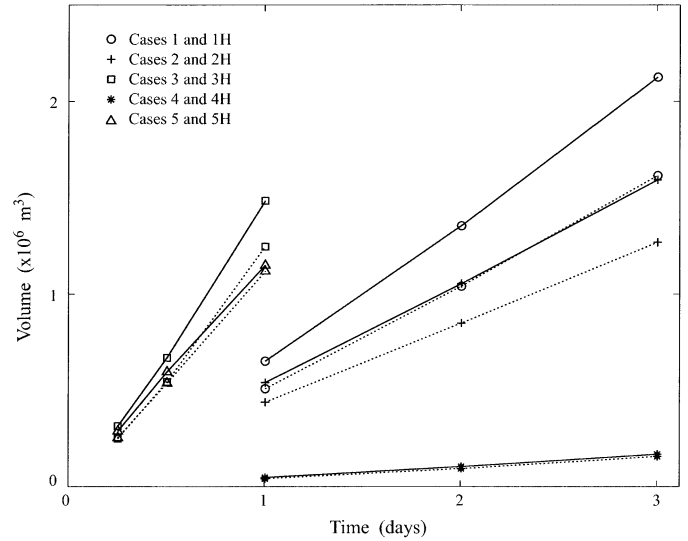

Fig. 10. Total volume of water per unit width with pH < 6, calculated after 1, 2, and 3 d (cases 1, 2, and 4) and after 6, 12, and 24 h for benthic storm cases (i.e., cases 3 and 5). Solid lines correspond to the cases with an absence of hydrate, whereas dotted lines are obtained for cases in which hydrate is present.

at the lake surface, and C_{amb} is the ambient concentration, which is negligible compared to C_0 when uptake kinetics are not limiting.

Integrating our results of CO_2 distribution until a steady state is achieved and using the known values of surface concentration and area, we can estimate V_p using Eq. 16. The dissolution rates derived for all cases are summarized in Table 3, which also contains time until complete dissolution of a liquid CO_2 lake assuming an initial depth of 50 m.

Table 3. Dissolution from the CO_2 lake. The second and the third columns are the piston velocity and the dissolution rate, respectively, derived for each of the corresponding cases given in the first column. Time of complete dissolution calculated for an initial lake depth of 50 m is given in the fourth column.

Case	V_p $(10^{-7}$ m s$^{-1})$	Dissolution rate (cm yr^{-1})	Time of complete dissolution* (yr)
1	8.5	169	29.6
1H	7.9	61	82.4
2	5	99	50.4
2H	4.8	37	135.6
3	22.6	450	11.1
3H	22.1	170	29.5
4	0.9	18	280.3
4H	1.6	12	407.7
5	16.0	317	15.8
5H	21.1	162	30.9

* Time of complete dissolution for the CO_2 lake with a surface area of 500 × 500 m² and an initial depth of 50 m, derived using Eq. 16. The total amount of liquid CO_2 in the lake is 1.31 × 10⁷ ton, using density of liquid CO_2 ~1,050 kg m^{-3} at ~5°C and ~3,000 m (*see Fig. 1*). This corresponds to 2.25 yr of emission from a 1 GW coal-fired power plant (~16,000 tons d^{-1}).

Discussion

Model results—The rate of dissolution of CO_2 from a liquid CO_2 source to the overlying deep ocean water is retarded when a thin hydrate film is present over the interface. This mechanism is significant when the change of water density is neglected in the model. The presence of the hydrate decreases the dissolution rate with a factor of 2.7, on average, over cases 1–3 (Table 3). However, when the increase in density of seawater enriched by dissolved CO_2 is taken into account, the stability increases at the expense of vertical mixing. In consequence, the dissolution is suppressed. A comparison of cases 2 and 4 shows that the dissolution rate is about 5.5 times larger in case 2 (density change effects neglected) than in case 4 (density change effects included). When the density effects are considered, the presence of the hydrate decreases the dissolution rate by a factor of 1.7, on average, over cases 4 and 5 (Table 3). This effect can also be seen in the total volume of water with pH < 6. Note that in Fig. 10 the corresponding volumes are not significantly larger for cases 4 and 5 than for cases 4H and 5H.

The dissolution rate obtained for case 4H, which represents a realistic situation in the deep ocean, can be compared to those measured in the field. Dunk et al.'s (unpubl.) estimate of 1.7 μmol cm^{-2} s^{-1} (*see* "Hydrate formation at liquid CO_2–water interface") is 170 times larger than 0.01 μmol cm^{-2} s^{-1} (derived from 12 cm yr^{-1} using the partial molar volume of CO_2 in seawater, $\bar{\nu} = 34 \times 10^{-6}$ m^3 mol^{-1}). This might, perhaps, be attributable to measurements that do not represent the steady state dissolution rate because Dunk et al. (unpubl.) only monitored for 15 min, probably when the mass transfer coefficient was considerably larger than a steady state value. Peltzer et al. (unpubl.) have measured the dissolution rate of liquid CO_2 in two separate experiments: first, by observing the slow decrease in the level of the liquid CO_2 pool using a time-lapse video camera system, and second, by observing the change in pH, measured 10 cm into the liquid CO_2 pool, as a function of time. Their results were 0.2 and 1.8 μmol cm^{-2} s^{-1}, respectively. Our model results at 1 h (i.e., before a steady state is achieved) yield a dissolution rate of 153 cm yr^{-1} (0.14 μmol cm^{-2} s^{-1}), which is of the same order of magnitude as the video observations and an order of magnitude less than the estimations through the pH observations. All determinations bear uncertainties, however, indicating that the dissolution rate might vary greatly.

Benthic storms—Episodic events of strong, bottom-intensified currents, called "benthic storms," have been observed in several places in the deep ocean—for example, the northeast Atlantic (Klein 1987), the Argentine Basin (Richardson et al. 1993), the tropical Pacific (Kontar and Sokov 1994), and the central Greenland Sea (Woodgate and Fahrbach 1999). In the deep northeast Atlantic, mean velocities near the bottom (<75 m above the bottom) ranged between 2 and 6 cm s^{-1}; however, benthic storms with duration of 3–25 d were observed with velocities >25 cm s^{-1}. The thickness of the BBL varied between 20 and 150 m, depending on the velocity. In the Greenland Sea, similar storms occurred with speeds reaching 43 cm s^{-1}, at 50 m above the sea floor, about

four times a year with a duration of about 1 week. The studies from the tropical Pacific revealed considerable eddy activity through the whole water column. The benthic storms were reported to be associated with these eddies. Hollister and McCave (1984) suggest that benthic storm events occur where there is (1) an overlying eddy system or strong surface current, (2) strong, permanent currents at depth, and (3) sediments that are easily brought into suspension. In our simulations of the cases representative of benthic storms, we used a mean velocity of 20 cm s^{-1} and a BBL thickness of 100 m, both in agreement with the observations. Our results show that the spatial distribution of dissolved CO_2 can cover the whole boundary layer and extend to about 20 km after 1 d. The dissolution rate can vary between ~1.6 and 4.5 m yr^{-1} (Table 3). The volume of water with low pH likely to affect the marine biota is ~2–10 times the amount calculated for cases without the storm (Fig. 10). The typical duration of such a storm of 1 week will inevitably damage the benthic life over considerable spatial extents. If benthic storms are related to eddies, Ekman pumping and nonzero vertical velocities can be expected. This has not been included in the present model experiments.

If we assume that the energetic eddies outside the boundary layer are at the same scale as the BBL thickness, h, and have an energy density of u^2, their kinetic energy per unit area and density is $K = \frac{1}{2}u^2h$. Assuming these eddies will completely mix a stratification $\Delta\rho$ over h, an energy of $\frac{1}{2}(g\Delta\rho/\rho)h^2$ is required. For $u = 20$ cm s^{-1}, $h = 100$ m and $\rho = 1{,}035$ kg m^{-3}; $K \approx 2$ W m^{-2} and can only mix a $\Delta\rho \approx 0.04$ kg m^{-3} over h. Thus, the enhanced density differences resulting from dissolution of CO_2 (Fig. 9a) provide for strong enough stratification to suppress the turbulence.

Instability at the hydrate membrane—The hydrate membrane is disrupted by the mean flow and the sweep of eddies from the adjacent turbulent region. The interface is subject to shear flow and therefore susceptible to Kelvin–Helmholtz (K-H) instability. When the surface tension is absent, the form of the instabilities is such that the shortest wavelength components of a perturbation grow the fastest (Turner 1973). The surface tension would limit this instability by providing an extra restoring force that will stabilize the high-wave number modes.

Consider the 2D motion of two immiscible, incompressible, inviscid fluids separated by a sharp interface in two horizontal, parallel streams of different velocities U_1 and U_2 and densities ρ_1 and ρ_2, where the faster and lighter stream is above the other. The shear layer appears as a vortex sheet inside an irrotational flow. Application of the linear stability analysis reveals that the flow is unstable if

$$(U_1 - U_2)^2 > 2\frac{(\rho_1 + \rho_2)}{\rho_1\rho_2}\{g\gamma(\rho_1 - \rho_2)\}^{1/2} \quad (17)$$

with a cutoff wavelength of

$$\lambda = \frac{2\pi}{k} = 2\pi\left\{\frac{\gamma}{g(\rho_1 - \rho_2)}\right\}^{1/2} \quad (18)$$

where γ is the interface tension and k is the wave number (Drazin and Reid 1981).

Aya et al. (1992) measured the tensile strength of CO$_2$ hydrate film as 1.3 N m^{-1} at 5 MPa and 6°C. This is about 17 times that of water at the same temperature. Recently, Yamane et al. (2000) conducted accurate laboratory measurements of the strength of the CO$_2$ hydrate membrane between liquid CO$_2$ and fresh/artificial seawater at 40–45 MPa using a Du-Nuoy–type surface tension meter. The membrane strength evaluated for freshwater, water with 0.5, 1, and 1.5 times the salinity of average seawater and temperatures within 1–6°C was reported to be ~0.1 N m^{-1}, whereas for temperatures greater than 6°C, an abrupt increase by an order of magnitude was observed.

Consider the case where a hydrate layer with a density of ρ_1 = 1,120 kg m^{-3} lies below a layer with ρ_2 = 1,050 kg m^{-3} (approximate density of seawater saturated with CO$_2$). Using γ = 0.1 N m^{-1} and g = 9.8 m s^{-2} and solving Eq. 17 for ($U_1 - U_2$) shows that the flow generates waves on the hydrate interface if the relative speed above the hydrate film exceeds 17 cm s^{-1}. A cutoff wavelength of 7.6 cm can be obtained from Eq. 18. It should be noted that the benthic storms are often associated with velocities greater than 20 cm s^{-1}. Thus, it might be expected that the episodic events can disrupt the hydrate layer through interfacial instabilities leading to bursts of enhanced CO$_2$ dissolution.

The reaction that forms hydrate is exothermic, and the release of heat and rejection of brine can generate local instabilities at the hydrate membrane. The enthalpy change of reaction (i.e., the difference between the overall enthalpy change and the heat of dissolution) is ~50 kJ mol^{-1} (Ohgaki et al. 1993). Aya et al. (1997) measured a temperature increase of $\Delta T \approx$ 2.2 K associated with hydrate formation during their experiments at 30 MPa using a simulation facility for a 3,000-m-deep ocean. Assuming that the hydrate film continuously decays and re-establishes on short time scales (Mori 1998), a quasi-steady state with constant buoyancy flux can be established. Double-diffusive instabilities can arise with "salt finger" or "diffusive" configurations that could lead to enhanced vertical mixing. Such instabilities have been observed in liquid metal, magma, heat-salt, sugar-salt, and semiconductor oxide regimes (Schmitt 1983), as well as aqueous solutions such as Na$_2$CO$_3$ (Turner 1996), which crystallized when cooled from the top.

Dense plume of CO$_2$-enriched seawater—It should be noted that even in the absence of an ambient flow, the dissolved CO$_2$ will create a dense plume of CO$_2$-enriched seawater, which can propagate as a gravity current, even on flat bottoms. The flow is driven by the difference in densities. This driving force is not included in the model.

Gravity currents have received considerable attention for both rotating and nonrotating systems, and extensive reviews can be found in Simpson (1987) and Turner (1986). The dynamics at and inside the front of a gravity current control the dynamics of the flow; this zone of intense mixing plays an important role in determining the flow rate. The most detailed experiments to describe the gravity currents flowing on surfaces covering a range of bottom slopes, $0° \leq \beta \leq 90°$, were reported by Britter and Linden (1980). They found, in particular, that for $\beta > 5°$, the mixing at the head increased dramatically with slope, whereas the velocity of the

head remained constant, at ~60% of the mean velocity of the following flow. However, for $\beta \leq 0.5°$, the current decelerates. On the other hand, in the limit $\beta \rightarrow 0$ and in the absence of mixing, the theory gives a critical slope of ~2C$_D$ to maintain a steady flow (for details, *see* the discussion in Britter and Linden 1980), where C$_D$ is the drag coefficient. Using C$_D$ = 2 × 10^{-3} (*see,* e.g., Elliott 1984), a slope of 4 × 10^{-3} can lead to a steady gravity current. This value is typical of the abyssal ocean.

K-H instabilities are likely to develop on the interface between the dense CO$_2$ plume and seawater (for the onset of instability and K-H–dominated behavior, *see* Thorpe 1973). In stratified conditions, the examination of the dispersion relation, deduced from the Taylor–Goldstein equation, suggests that Holmboe instability (Holmboe 1962) occurs, provided the Schmidt number, Sc, is significantly large (>100 according to Smyth and Peltier 1991). This generates a situation in which gradients in density are significantly more important than those in velocity. For the CO$_2$–seawater system, Sc = O(1,000), and we can expect Holmboe instability to develop. Physically, it appears like two trains of waves that propagate in opposite directions on the opposite sides of the density interface. Similar instabilities have been observed in stratified exchange flows (Pawlak and Armi 1996).

The dissolution of liquid CO$_2$ deposited at the bottom of the deep ocean is a complex phenomenon. The buoyancy behavior of the CO$_2$ hydrate, its density, and its mechanical properties are not thoroughly understood yet. Our calculations are based on the best available hydrate model formulation coupled to a BBL mixing parameterization and give dissolution rates that are initially comparable to those estimated from short-duration field experiments, but with steady state values one to two orders of magnitude smaller. The added anthropogenic CO$_2$ to the ambient water will change the CO$_2$ chemistry in the ocean by reducing the pH at the site. The resulting low pH values obtained by altering the carbonic acid system in seawater will have severe effects on the ecosystem (Seibel and Walsh 2001) and inevitably wipe out the benthic life in the vicinity. The interface between the liquid CO$_2$ lake and the hydrate film, as well as that between the dense, CO$_2$-enriched seawater plume and ambient water, could undergo various types of instabilities that could enhance the mixing rate. Further experimental and theoretical work is merited on the small-scale mechanisms likely to affect the hydrate membrane, as well as larger scale processes affecting the dense CO$_2$-enriched plume, in order to achieve predictions of higher reliability.

References

ALENDAL, G., AND H. DRANGE. 2001. Two-phase, near field modeling of purposefully released CO$_2$ in the ocean. J. Geophys. Res. **106:** 1085–1096.

ARMI, L., AND R. C. MILLARD. 1976. The bottom boundary layer of the deep ocean. J. Geophys. Res. **81:** 4983–4990.

———. 1977. The dynamics of the bottom boundary layer of the deep ocean, p. 153–164. *In* C. J. J. Nihoul [ed.], Bottom turbulence. 8th International Liège Colloquium on Ocean Hydrodynamics. Elsevier Scientific.

———. 1978. Some evidence for boundary mixing in the deep ocean. J. Geophys. Res. **83:** 1971–1979.

AYA, I., K. YAMANE, AND N. YAMADA. 1992. Stability of clathrate-hydrate of carbon dioxide in highly pressurized water, p. 17–22. *In* P. G. Kroeger and Y. Bayazitoglu [eds.], Fundamentals of phase change: Freezing, melting and sublimation. American Society of Mechanical Engineers.

———, ———, AND H. NARIAI. 1997. Solubility of CO_2 and density of CO_2 hydrate at 30 MPa. Energy **22:** 263–271.

BISHNOI, P. R., AND D. B. ROBINSON. 1971. An evaluation of methods for determining the parameters in BWR equation of state using volumetric and heat capacity data. Can. J. Chem. Eng. **49:** 642–650.

BREWER, P. G., G. FRIEDERICH, E. T. PELTZER, AND F. M. ORR, JR. 1999. Direct experiments on the ocean disposal of fossil fuel CO_2. Science **284:** 943–945.

BRITTER, R. E., AND P. F. LINDEN. 1980. The motion of the front of a gravity current traveling down an incline. J. Fluid Mech. **99:** 531–543.

CLAUSER, F. H. 1956. The turbulent boundary layer. Adv. Appl. Mech. **4:** 1–51.

D'ASARO, E. 1982. Velocity structure of the benthic ocean. J. Phys. Oceanogr. **12:** 313–322.

DRANGE, H., G. ALENDAL, AND P. M. HAUGAN. 1993. A bottom gravity current model for CO_2-enriched seawater. Energy Convers. Manag. **34:** 1065–1072.

DRAZIN, P. G., AND W. H. REID. 1981. Hydrodynamic stability. Cambridge Univ. Press.

ELLIOTT, A. J. 1984. Measurements of turbulence in an abyssal boundary layer. J. Phys. Oceanogr. **14:** 1779–1786.

FER, I., U. LEMMIN, AND S. A. THORPE. 2001. Cascading of water down the sloping sides of a deep lake in winter. Geophys. Res. Lett. **28:** 2093–2096.

———, ———, AND ———. 2002*a*. Observations of mixing near the sides of a deep lake in winter. Limnol. Oceanogr. **47:** 535–544.

———, ———, AND ———. 2002*b*. Winter cascading of cold water in Lake Geneva. J. Geophys. Res. **107:** C6, 3060, 10.1029/2001JC000828.

FERZIGER, J. H., AND M. PERIĆ. 1999. Computational methods for fluid dynamics. Springer-Verlag.

FISCHER, H. B. 1973. Longitudinal dispersion and turbulent mixing in open-channel flow. Annu. Rev. Fluid Mech. **5:** 59–78.

GARRETT, C. 1990. The role of secondary circulation in boundary mixing. J. Geophys. Res. **95:** 3181–3188.

———. 2001. An isopycnal view of near-boundary mixing and associated flows. J. Phys. Oceanogr. **31:** 138–142.

GIGGENBACH, W. F. 1990. Water and gas chemistry of Lake Nyos and its bearing on the eruptive process. J. Volcanol. Geotherm. Res. **42:** 337–362.

HANDA, N., AND T. OHSUMI [EDS.]. 1995. Direct ocean disposal of carbon dioxide. TERRAPUB.

HAUGAN, P. M., AND H. DRANGE. 1992. Sequestration of CO_2 in the deep ocean by shallow injection. Nature **357:** 318–320.

HINZE, J. O. 1975. Turbulence. McGraw-Hill.

HOLLISTER, C. D., AND I. N. MCCAVE. 1984. Sedimentation under deep-sea storms. Nature **309:** 220–225.

HOLMBOE, J. 1962. On the behavior of symmetric waves in stratified shear layers. Geophys. Publ. **24:** 67–113.

HONDA, M., J. HASHIMOTO, J. NAKA, AND H. HOTTA. 1995. CO_2 hydrate formation and inversion of density between liquid CO_2 and H_2O in deep sea: Experimental study using submersible 'Shinkai 6500', p. 35–43. *In* N. Handa and T. Ohsumi [eds.], Direct ocean disposal of carbon dioxide. TERRAPUB.

HOUGHTON, J. T., AND OTHERS [EDS.]. 1995. Climate change 1994.

Radiative forcing of climate change and an evaluation of the IPCC IS92 emission scenarios. Cambridge Univ. Press.

INOUE, Y., K. OHGAKI, Y. HIRATA, AND E. KUNUGITA. 1996. Numerical study on effects of hydrate formation on deep sea CO_2 storage. J. Chem. Eng. Jpn. **29:** 648–655.

KING, M. B. 1969. Phase equilibrium in mixtures. Pergamon.

KLEIN, H. 1987. Benthic storms, vortices, and particle dispersion in the deep west European basin. Dtsch. Hydrogr. Z. **40:** 87–102.

KONTAR, E. A., AND A. V. SOKOV. 1994. A benthic storm in the northeastern tropical Pacific over the fields of manganese nodules. Deep-Sea Res. I **41:** 1069–1089.

LEDWELL, J. R., E. T. MONTGOMERY, K. L. POLZIN, L. C. S. LAURENT, R. W. SCHMITT, AND J. M. TOOLE. 2000. Evidence for enhanced mixing over rough topography in the abyssal ocean. Nature **403:** 179–182.

LIDE, D. R. 2000. CRC handbook of chemistry and physics. CRC Press.

LILLY, D. K., D. E. WACO, AND S. I. ADELFANG. 1974. Stratospheric mixing estimated from high-altitude turbulence measurements. J. Appl. Meteorol. **13:** 488–493.

LIRO, C., E. E. ADAMS, AND H. J. HERZOG. 1992. Modelling the release of CO_2 in the deep ocean. Energy Convers. Manag. **5–8:** 667–674.

MARCHETTI, C. 1977. On geoengineering and the CO_2 problem. Clim. Chang. **1:** 59–68.

MITSUBISHI, J. K. K. 1990. Method for the fixation of carbon dioxide, apparatus for fixing and disposing carbon dioxide, and apparatus for the treatment of carbon dioxide. European Patent Application, 90250288.9.

MORI, Y. H. 1998. Clathrate hydrate formation at the interface between liquid CO_2 and water phases—a review of rival models characterizing 'hydrate films'. Energy Convers. Manag. **39:** 1537–1557.

———, AND T. MOCHIZUKI. 1997. Mass transport across clathrate hydrate films—a capillary permeation model. Chem. Eng. Sci. **52:** 3613–3616.

———, AND ———. 1998. Dissolution of liquid CO_2 into water at high pressures: A search for the mechanism of dissolution being retarded through hydrate-film formation. Energy Convers. Manag. **39:** 567–578.

MUNK, W. H. 1966. Abyssal recipes. Deep-Sea Res. **13:** 707–730.

OAKEY, N. S. 1982. Determination of the rate of dissipation of turbulent energy from simultaneous temperature and velocity shear microstructure measurements. J. Phys. Oceanogr. **12:** 256–271.

OHGAKI, K., Y. MAKIHARA, AND K. TAKANO. 1993. Formation of CO_2 hydrate in pure and seawaters. J. Chem. Eng. Jpn. **26:** 558–564.

OHSUMI, T. 1993. Prediction of solute carbon dioxide behaviour around a liquid carbon dioxide pool on deep ocean basin. Energy Convers. Manag. **34:** 1059–1064.

———, N. NAKASHIKI, K. SHITASHIMA, AND K. HIRAMA. 1992. Density change of water due to dissolution of carbon dioxide and near-field behavior of CO_2 from a source on deep-sea floor. Energy Convers. Manag. **33:** 685–690.

OSBORN, T. R. 1980. Estimates of the rate of vertical diffusion from dissipation measurements. J. Phys. Oceanogr. **10:** 83–89.

PAWLAK, G., AND L. ARMI. 1996. Stability and mixing of a two layer exchange flow. Dyn. Atmos. Oceans **24:** 139–151.

PELTZER, E. T., P. G. BREWER, G. FRIEDERICH, AND G. REHDER. 2000. Direct observation of the fate of oceanic carbon dioxide release at 800 m. Am. Chem. Soc., Div. Fuel Chem. **45:** 794–798.

POLZIN, K. L., K. G. SPEER, J. M. TOOLE, AND R. W. SCHMITT. 1996. Intense mixing of Antarctic bottom water in the equatorial Atlantic Ocean. Nature **380:** 54–57.

RICHARDSON, M. J., G. L. WEATHERLY, AND W. D. GARDNER. 1993. Benthic storms in the Argentine Basin. Deep-Sea Res. II **40:** 975–987.

SAKAI, H., AND OTHERS. 1990. Venting of carbon dioxide-rich fluid and hydrate formation in mid-Okinawa Trough Backarc Basin. Science **248:** 1093–1096.

SAUNDERS, P. M. 1983. Benthic observations on the Madeira Abyssal Plain: Currents and dispersion. J. Phys. Oceanogr. **13:** 1416–1429.

SCHMITT, R. W. 1983. The characteristics of salt fingers in a variety of fluid systems, including stellar interiors, liquid metals, oceans and magmas. Phys. Fluids **26:** 2373–2377.

SEIBEL, B. A., AND P. J. WALSH. 2001. Carbon cycle—potential, impacts of CO₂ injection on deep-sea biota. Science **294:** 319–320.

SHINDO, Y., Y. FUJIOKA, Y. YANAGISHITA, T. HAKUTA, AND H. KOMIYAMA. 1995. Formation and stability of CO₂ hydrate, p. 217–231. *In* N. Handa and T. Ohsumi [eds.], Direct ocean disposal of carbon dioxide. TERRAPUB.

SIMPSON, J. E. 1987. Gravity currents: In the environment and the laboratory. Ellis Horwood series in environmental science. Ellis Horwood.

SMYTH, W. D., AND W. R. PELTIER. 1991. Instability and transition in finite-amplitude Kelvin–Helmholtz and Holmboe waves. J. Fluid Mech. **228:** 387–415.

STEWART, P. B., AND P. MUNJAL. 1970. Solubility of carbon dioxide in pure water, synthetic sea water, and synthetic sea water concentrates at 5 degrees to 2K degrees C and 10-atm to 45-atm pressure. J. Chem. Eng. Data **15:** 67.

TENG, H., S. M. MASUTANI, C. M. KINOSHITA, AND G. C. NIHOUS. 1996*a.* Solubility of CO₂ in the ocean and its effect on CO₂ dissolution. Energy Convers. Manag. **37:** 1029–1038.

———, A. YAMASAKI, AND Y. SHINDO. 1996*b.* Stability of the hydrate layer formed on the surface of a CO₂ droplet in high-pressure, low-temperature water. Chem. Eng. Sci. **51:** 4979–4986.

THORPE, S. A. 1973. Experiments on instability and turbulence in a stratified shear flow. J. Fluid Mech. **61:** 731–751.

———. 1987. Current and temperature variability on the continental slope. Philos. Trans. R. Soc. Lond., A **323:** 471–517.

———, P. HALL, AND M. WHITE. 1990. The variability of mixing at the continental slope. Philos. Trans. R. Soc. Lond., A **331:** 183–194.

TOOLE, J. M., AND J. T. MCDOUGALL. 2001. Mixing and stirring in the ocean interior, p. 337–355. *In* G. Siedler, J. Church, and J. Gould [eds.], Ocean circulation and climate. Observing and modelling the global ocean. Academic.

———, R. W. SCHMITT, AND K. L. POLZIN. 1997. Near-bottom mixing above the flanks of a midlatitude seamount. J. Geophys. Res. **102:** 947–959.

TURNER, J. S. 1973. Buoyancy effects in fluids. Cambridge Univ. Press.

———. 1986. Turbulent entrainment: The development of the entrainment assumption, and its application to geophysical flows. J. Fluid Mech. **173:** 431–471.

———. 1996. Laboratory models of double-diffusive processes. *In* A. Brandt and H. J. S. Fernando [eds.], Double diffusive convection. American Geophysical Union.

UCHIDA, T. 1997. Physical property measurements on CO₂ clathrate hydrates. Review of crystallography, hydration number, and mechanical properties. Waste Manag. **17:** 343–352.

UDACHIN, K. A., C. I. RATCLIFFE, AND J. A. RIPMEESTER. 2001. Structure, composition, and thermal expansion of CO₂ hydrate from single crystal X-ray diffraction measurements. J. Phys. Chem. B **105:** 4200–4204.

[UNESCO] UNITED NATIONS EDUCATIONAL, SCIENTIFIC, AND CULTURAL ORGANIZATION. 1981. Tenth report of the joint panel on oceanographic tables and standards. Technical Paper in Marine Sciences, 36.

VUKALOVICH, M. P., AND V. V. ALTUNIN. 1968. Thermophysical properties of carbon dioxide. Collets.

WEATHERLY, G. L. 1975. A numerical study of time-dependent turbulent Ekman layers over horizontal and sloping bottoms. J. Phys. Oceanogr. **5:** 288–299.

———, AND P. J. MARTIN. 1978. On the structure and dynamics of the ocean bottom boundary layer. J. Phys. Oceanogr. **8:** 557–570.

WEISS, R. F. 1974. Carbon dioxide in water and seawater: The solubility of a non-ideal gas. Mar. Chem. **2:** 203–215.

WIMBUSH, M., AND W. H. MUNK. 1970. The benthic boundary layer, p. 731–758. *In* M. N. Hill [ed.], The Sea. Wiley.

WOODGATE, R. A., AND E. FAHRBACH. 1999. Benthic storms in the Greenland sea. Deep-Sea Res. I **46:** 2109–2127.

YAMANE, K., I. AYA, S. NAMIE, AND H. NARIAI. 2000. Strength of CO₂ hydrate membrane in sea water at 40 MPa. Ann. N.Y. Acad. Sci. **912:** 254–260.